

RESEARCH ARTICLE | OCTOBER 23 2024

Photoacoustic spectroscopy with a widely tunable narrowband fiber-feedback optical parametric oscillator

Luca Schmid ; Florent Kadriu ; Sandro Kuppel ; Moritz Floess ; Tobias Steinle; Harald Giessen 

AIP Advances 14, 105328 (2024)

<https://doi.org/10.1063/5.0212392>

Articles You May Be Interested In

Coherent detection of pulsed narrowband terahertz radiation

Appl. Phys. Lett. (January 2006)

Passive depth estimation for a narrowband source using a single vector sensor in deep water

JASA Express Lett. (June 2023)

Time-reversible and fully time-resolved ultra-narrowband biphoton frequency combs

AIP Advances

Why Publish With Us?



19 DAYS
average time
to 1st decision



500+ VIEWS
per article (average)



INCLUSIVE
scope

[Learn More](#)



Photoacoustic spectroscopy with a widely tunable narrowband fiber-feedback optical parametric oscillator

Cite as: AIP Advances 14, 105328 (2024); doi: 10.1063/5.0212392

Submitted: 30 May 2024 • Accepted: 4 October 2024 •

Published Online: 23 October 2024




View Online



Export Citation



CrossMark

Luca Schmid,^{1,a)}  Florent Kadriu,^{1,2}  Sandro Kuppel,^{1,2}  Moritz Floess,¹  Tobias Steinle,^{1,2} and Harald Giessen^{1,2} 

AFFILIATIONS

¹4th Physics Institute and Research Center SCoPE, University of Stuttgart, Pfaffenwaldring 57, 70569 Stuttgart, Germany

²SI Stuttgart Instruments GmbH, Curiestraße 2, 70563 Stuttgart, Germany

^{a)} Author to whom correspondence should be addressed: luca.schmid@pi4.uni-stuttgart.de

ABSTRACT

Trace gas analysis is a key tool for the investigation of man-made environmental pollution as well as for early detection of respiratory diseases. To detect tiny concentrations, sensitive methods such as cavity ring down spectroscopy or plasmonic sensors have been used. Here, we demonstrate the combination of the photoacoustic effect in a classical cell with a novel, rapidly tunable, narrowband fiber-feedback optical parametric oscillator. The high sensitivity of photoacoustic cells and the extremely narrow linewidth as well as the wide and rapid tunability of the fiber-feedback optical parametric oscillator enable a high resolution of the rotational and vibrational bands of molecules in the near-infrared region. Photoacoustic spectra of methane, carbon dioxide, and water at ambient pressure are obtained in a broad spectral range and compared to high-resolution transmission molecular absorption database. In particular, scanning the entire carbon dioxide overtone around 4965 cm^{-1} at 2000 ppm takes 185 s with a signal-to-noise ratio of 31. This approach enables a wide tunability in the entire near- and mid-infrared spectral region suitable for many environmental and medical applications.

© 2024 Author(s). All article content, except where otherwise noted, is licensed under a Creative Commons Attribution (CC BY) license (<https://creativecommons.org/licenses/by/4.0/>). <https://doi.org/10.1063/5.0212392>

I. INTRODUCTION

Gas sensing poses different obstacles for respective applications. Hence, multiple methods and sensors have been optimized, such as nanoantenna-enhanced gas sensors,¹ FTIR,² or cavity ring down spectroscopy.³ Since the discovery that light could be used to create sound,⁴ the photoacoustic effect has become an important tool for trace gas sensing. To exploit its full potential by adding spectral selectivity, multi-wavelength or tunable light sources such as frequency combs,⁵⁻⁷ quantum cascade lasers,⁸ intraband cascade lasers, and optical parametric oscillator (OPO) are commonly utilized. In photoacoustic cells also, the way of sensing has been further developed. Cantilever-⁹ and quartz-enhanced^{10,11} photoacoustic measurements are the preferred ways. In most cases, the required resolution, the dynamic range of the absorption features, or the required wavelength range are limited due to the inherent properties of available light sources. To overcome these challenges, one needs to achieve a broad accessible wavelength range with narrow

linewidths for maximum resolution, combined with the ability for fast sweeping. Currently, the only way to produce tunable radiation over a spectral range spanning several octaves is optical parametric frequency conversion.

Here, we employ a fiber-feedback OPO (FFOPO), optimized for narrowband operation that is ideally suited to fulfill the mentioned criteria.^{12,13} We demonstrate rotational vibrational spectroscopy of methane, carbon dioxide, and water. This is realized by the combination of a microphone-based photoacoustic cell with a widely tunable FFOPO (1450 nm up to 4000 nm). This combination enables high sensitivity in linewidth, the detection of concentrations in the ppm range, and a wide dynamic range for measuring the absorption.

II. SETUP

The centerpiece of the setup is an H-type photoacoustic cell, which contains a cylindrical resonator with a length of 80 mm,

a diameter of 14 mm, and a quality factor of 20. The buffer volume at each end is 113 cm^3 . A schematic of the setup is depicted in Fig. 1(a). Molecules are excited inside the cell when the wavelength is matched to an absorption feature. For the excitation of standing acoustic waves, we modulate the light with the resonance frequency of the resonator. The experimentally measured resonance frequency is $f_{\text{mod}} \approx 1996 \text{ Hz}$. The FFOPO (Stuttgart Instruments *Piano* prototype) is spectrally tunable, and the laser output is modulated by a chopper wheel. This frequency is matched to the cell resonance and used for demodulation with a lock-in amplifier. The amplitudes of standing acoustic waves are measured with a microphone. The microphone is positioned at the midpoint of the resonator to read out the first longitudinal mode.¹⁴ By sweeping the wavelength of the laser through the spectrum while keeping the modulation frequency constant, an absorption signal is generated at each corresponding wavelength. The FFOPO is tunable from 1450 nm up to 4000 nm and calibrated to emit a constant output power of 100 mW in the FFOPO signal range (1450 to $\sim 2100 \text{ nm}$). The measured linewidths from 1830 to 2030 nm are displayed in Fig. 1(b), where the spectral linewidth for the 1930 nm measurement is depicted in more detail with an FWHM of 0.24 nm (0.65 cm^{-1}).

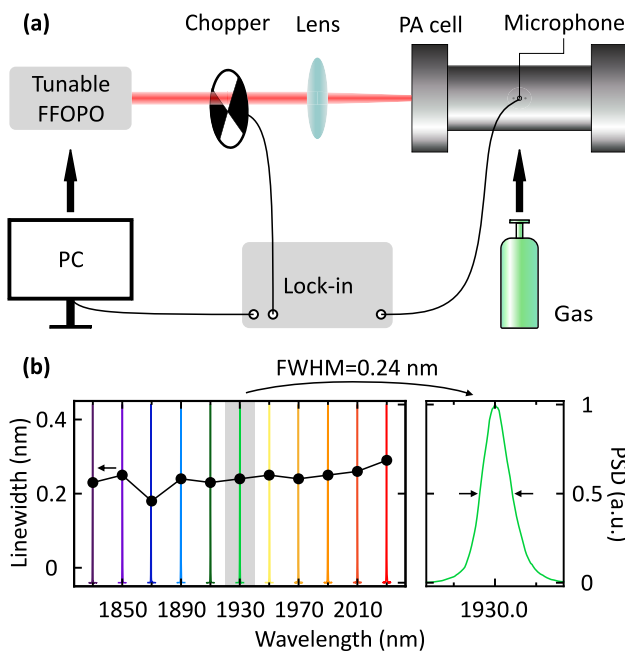


FIG. 1. Photoacoustic setup and spectral linewidths of the FFOPO. (a) Schematic of the setup with the photoacoustic cell. For the excitation of standing acoustic waves, the beam of the FFOPO is modulated with a mechanical chopper wheel and then focused into the cell. The tunable FFOPO is controlled by a PC. A microphone is positioned directly on the surface of the cylindrical resonator at its midpoint along the cylindrical axis. For a low noise signal, the absorption amplitude to the corresponding wavelength of the microphone signal is demodulated with the frequency of the chopper wheel. (b) Spectral power density of the laser system and corresponding FWHM of the spectra. The right plot illustrates the Gaussian shape of the spectrum at an FWHM linewidth of 0.24 nm (0.65 cm^{-1}).

III. RESULTS AND DISCUSSION

The calculated absorption spectra for methane, carbon dioxide, and water in the accessible wavelength range of the FFOPO are displayed in Fig. 2. The observed regions are around 3000, 5000, and 5300 cm^{-1} . The methane absorption band is strong, and single lines are well visible in a wide frame of roughly 2550 nm ($\approx 4400 \text{ cm}^{-1}$) bandwidth. In comparison, the water absorption band around 5300 cm^{-1} is clearly weaker. The extremely weak overtone of carbon dioxide (see the inset) is roughly a factor of 350 times weaker than the highest methane absorption line.

The photoacoustic spectra are shown in Fig. 3, where the colored curves plot the measured data. In the first row, the measured signal compared to high-resolution transmission molecular absorption (HITRAN) data is shown,¹⁵ while the second row depicts the data compared to the convolved HITRAN data. The simulated data are convolved¹⁶ with a Gaussian spectral shape, where the full width at half maximum is set to the spectral width of the laser system. This allows a more quantitative comparison between theory and experiment. Row three displays zoom-ins of the highlighted areas of the second row. The methane (green) absorption spectrum, over 393 nm ($\approx 320 \text{ cm}^{-1}$) bandwidth shown in Fig. 3(a), is generated within a 450 s scan. This range is measured in the idler range of the FFOPO. For the convolution, a linewidth of 1.2 cm^{-1} ($\approx 1.3 \text{ nm}$) is used. For carbon dioxide (orange), the sweep of 37 nm ($\approx 70 \text{ cm}^{-1}$) took 185 s, which is illustrated in Fig. 3(b). The used spectral width for the convolution is 0.9 cm^{-1} ($\approx 0.4 \text{ nm}$). Even extremely weak absorption bands can be resolved. Taking the linewidth into account, we demonstrate that the convolved data are in good agreement with the measured data. The measured absorption of water in ambient air (blue), roughly at a concentration of 4840 ppm, is presented in Fig. 3(c). The full sweep over 110 nm ($\approx 300 \text{ cm}^{-1}$) is carried out in 330 s. For the convolution, an FWHM of 0.7 cm^{-1} ($\approx 0.25 \text{ nm}$) for the Gaussian spectrum is used. The signal-to-noise ratio (SNR) values at the maximum signal resonances are 368 (methane), 31 (carbon dioxide), and 1018 (water). The exploded views, the bottom row of Fig. 3, provide confirmation of the congruity between the relative strengths of the absorption features and their positions. For methane and water, the linewidth is no limiting factor. However, for the carbon dioxide spectrum, it is visible that the resolvable spectrum becomes less sharp because the absorption lines are located very close to each other. The linearity of the photoacoustic signal with increasing output power of the laser system is displayed in Fig. 4. For all three different species, the photoacoustic signal is measured for different optical powers of the FFOPO up to 200 mW. The absorption cross sections of the molecules are denoted in Table I. All three species could be detected using their overtones with strongly varying signal strengths, providing an indication of the dynamic range of the system. The background noise level of 0.06 mV, highlighted in light red in Fig. 4, is measured at a lock-in time constant of 40 ms. The noise level is mostly induced mechanically by the chopper wheel and does not further reduce for larger time constants. We estimate the signal-to-noise ratio by dividing the photoacoustic signal obtained at the most prominent absorption features by the above-mentioned noise floor of 0.06 mV. The signal strengths for different species are taken from Fig. 4 at 200 mW. Detection limits are calculated by assuming linear behavior between the concentration, the signal strength, and the strongest measured absorption line from Table I. Dividing the

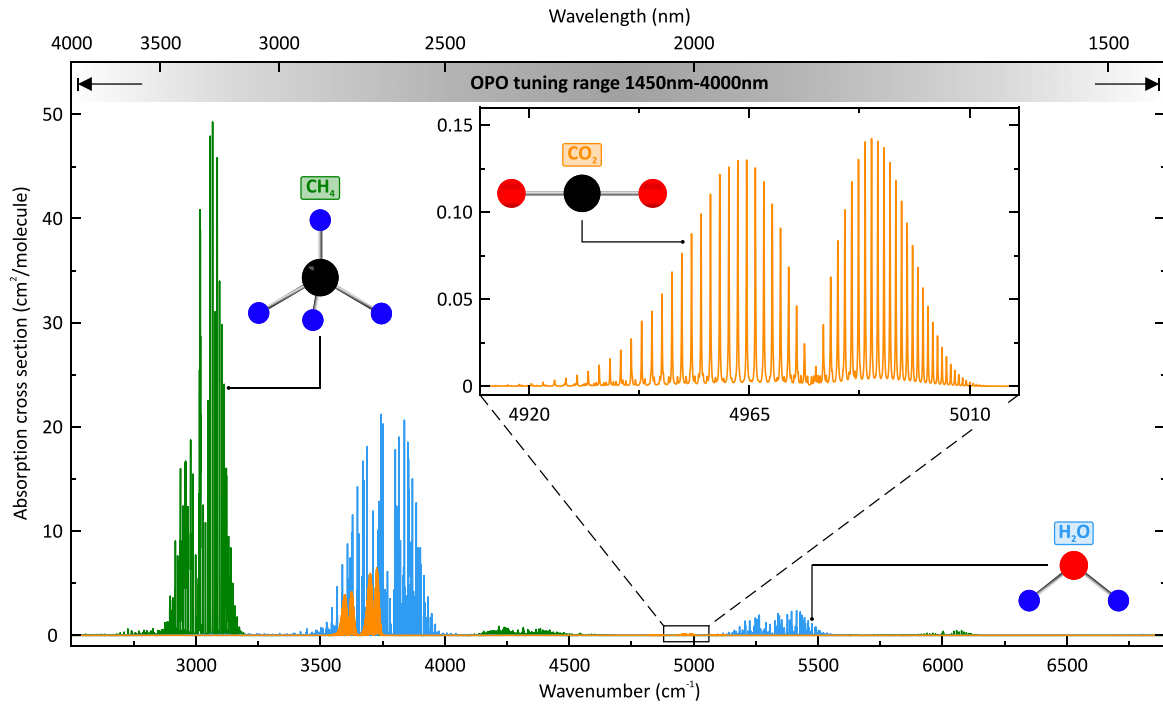


FIG. 2. The absorption cross sections calculated with HITRAN for methane, water, and carbon dioxide in the accessible wavelength range of the laser system. An extremely weak overtone of carbon dioxide around 4965 cm⁻¹ is displayed in the inset, which in comparison to the other absorption bands is almost not visible and a factor of 350 weaker than the strongest absorption line of the methane band at roughly 3000 cm⁻¹.

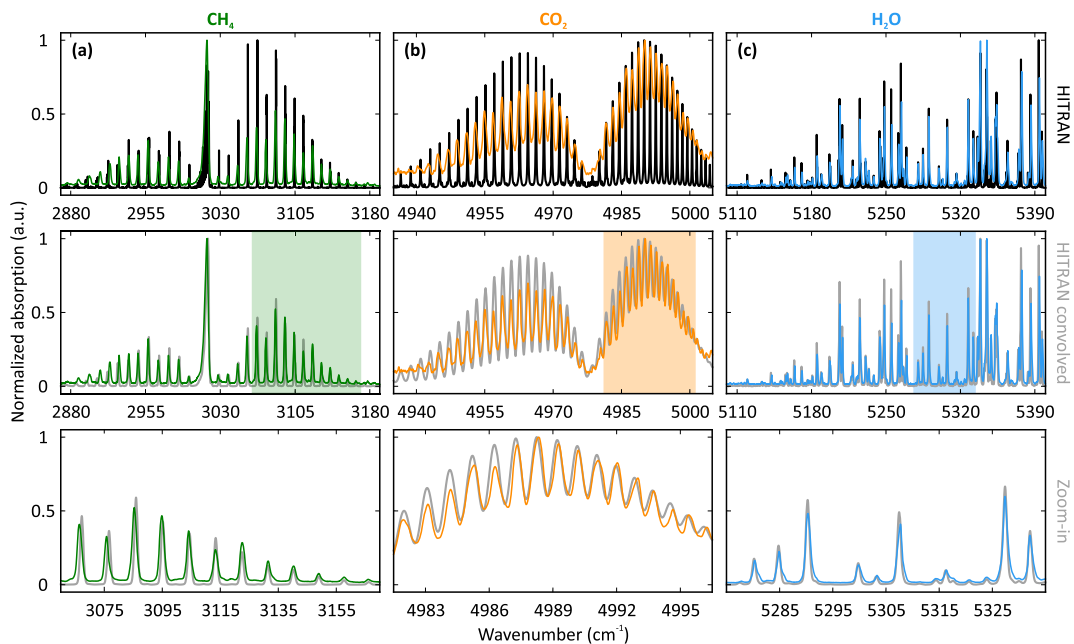


FIG. 3. Measured normalized absorption compared to HITRAN data and convolved HITRAN data. (a) Measured absorption of 200 ppm methane (in nitrogen), (b) 2000 ppm carbon dioxide (in nitrogen), and (c) water in ambient air (4840 ppm). In the first row, the measured data are compared to the HITRAN absorption cross sections while in the second row, HITRAN data are convolved with the spectral linewidths of the respective of the range. A zoom-in of the convolved data is shown below for the color deposited areas. All data are acquired with a constant laser input power of 100 mW.

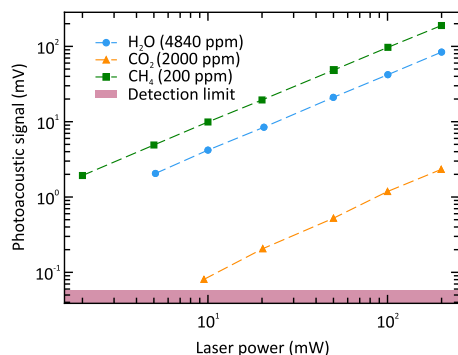


FIG. 4. Linearity of the photoacoustic signal and the laser power. Measured photoacoustic signal for the investigated concentrations of water, carbon dioxide, and methane as a function of the output power of the laser system. The detection limit due to the background noise of the photoacoustic setup is 0.06 mV measured at a lock-in time constant of 40 ms.

TABLE I. Detection limits of water (4840 ppm), carbon dioxide (2000 ppm), and methane (200 ppm) located at the strongest measured photoacoustic resonance and their corresponding absorption coefficients.

Molecule	H ₂ O	CO ₂	CH ₄
Wavenumber (cm ⁻¹)	5344.5	4990.0	3016.5
Abs. coefficient (cm ⁻¹)	1.83	0.14	40.82
SNR	1446	40	3258
Detection limit (ppm)	3	50	0.06

measured concentration by the obtained SNR will result in the detection limits for the molecules. We obtain a detection limit of 3 ppm for water, 50 ppm for carbon dioxide, and 60 ppb for methane.

IV. CONCLUSION

We have successfully demonstrated the measurement of trace gases at ppm concentrations with low detection time due to the combination of a photoacoustic cell and a widely tunable narrowband optical parametric oscillator as the laser source. Full absorption spectra of different strengths can be obtained within a few minutes. A high resolution of the relative strengths and the positions of the absorption lines are achieved for methane, carbon dioxide, and water. In comparison to the state of the art distributed feedback lasers, quantum cascade lasers, or nanosecond OPO systems, we combine an extremely broad tunability range with fast tuning and very high spectral density in a spectrally narrow beam.

Enhancing the setup with faster scan-rates and more power for monitoring concentration changes of various trace gases in real-time would be beneficial for tracking highly polluted areas, such as those in traffic jams. With the combination of photoacoustic and widely tunable narrowband OPOs, it is possible to determine the composition of mixtures precisely. Precaution supporting measures of Lung cancer, which has a high mortality rate, could benefit from such measurements.¹⁷ Decomposing arbitrary gas mixtures completely would allow measurement of the concentration of exact amounts of “false”

molecules that the lung produces and, therefore, detection of the disease at an early stage. The wide tunability as well as the stability and the excellent beam profiles of FFOPOs could exploit its full potential in imaging applications.

ACKNOWLEDGMENTS

L.S. would like to thank Ralph Gäbler for providing the photoacoustic cell and sharing his experiences with it. This study was supported by Carl-Zeiss-Stiftung; Deutsche Forschungsgemeinschaft (DFG, German Research Foundation), Grant No. 431314977/GRK2642; Center for Integrated Quantum Science and Technology (IQST); Baden-Württemberg Stiftung; Bundesministerium für Bildung und Forschung (KMU MIRSWEEP).

AUTHOR DECLARATIONS

Conflict of Interest

The authors have no conflicts to disclose.

Author Contributions

Luca Schmid: Formal analysis (lead); Investigation (equal); Methodology (equal); Validation (lead); Visualization (lead); Writing – original draft (equal); Writing – review & editing (equal). **Florent Kadriu:** Investigation (equal); Methodology (equal). **Sandro Kuppel:** Formal analysis (supporting); Software (lead). **Moritz Floess:** Methodology (supporting); Validation (supporting); Visualization (supporting). **Tobias Steinle:** Conceptualization (equal); Methodology (equal); Project administration (equal); Supervision (equal); Writing – original draft (equal); Writing – review & editing (equal). **Harald Giessen:** Conceptualization (equal); Funding acquisition (lead); Project administration (equal); Resources (lead); Supervision (equal); Writing – original draft (equal); Writing – review & editing (equal).

DATA AVAILABILITY

The data that support the findings of this study are available from the corresponding author upon reasonable request.

REFERENCES

- N. Liu, M. L. Tang, M. Hentschel, H. Giessen, and A. P. Alivisatos, “Nanoantenna-enhanced gas sensing in a single tailored nanofocus,” *Nat. Mater.* **10**, 631–636 (2011).
- C. Lindner, J. Kunz, S. J. Herr, S. Wolf, J. Kießling, and F. Kühnemann, “Nonlinear interferometer for Fourier-transform mid-infrared gas spectroscopy using near-infrared detection,” *Opt. Express* **29**, 4035–4047 (2021).
- G. Berden, R. Peeters, and G. Meijer, “Cavity ring-down spectroscopy: Experimental schemes and applications,” *Int. Rev. Phys. Chem.* **19**, 565–607 (2000).
- A. G. Bell, “LXVIII. Upon the production of sound by radiant energy,” *London, Edinburgh Dublin Philos. Mag. J. Sci.* **11**, 510–528 (1881).
- I. Sadiq, T. Mikkonen, M. Vainio, J. Toivonen, and A. Foltynowicz, “Optical frequency comb photoacoustic spectroscopy,” *Phys. Chem. Chem. Phys.* **20**, 27849–27855 (2018).

- ⁶M. A. Abbas, Q. Pan, J. Mandon, S. M. Cristescu, F. J. M. Harren, and A. Khodabakhsh, "Time-resolved mid-infrared dual-comb spectroscopy," *Sci. Rep.* **9**, 17247 (2019).
- ⁷J. T. Friedlein, E. Baumann, K. A. Briggman, G. M. Colacion, F. R. Giorgetta, A. M. Goldfain, D. I. Herman, E. V. Hoenig, J. Hwang, N. R. Newbury, E. F. Perez, C. S. Yung, I. Coddington, and K. C. Cossel, "Dual-comb photoacoustic spectroscopy," *Nat. Commun.* **11**, 3152 (2020).
- ⁸W. Ren, W. Jiang, N. P. Sanchez, P. Patimisco, V. Spagnolo, C.-e. Zah, F. Xie, L. C. Hughes, R. J. Griffin, and F. K. Tittel, "Hydrogen peroxide detection with quartz-enhanced photoacoustic spectroscopy using a distributed-feedback quantum cascade laser," *Appl. Phys. Lett.* **104**, 041117 (2014).
- ⁹H. Karlsson and S. Sinisalo, "Air quality monitoring with photoacoustic spectroscopy," *Opt. Photonik* **12**, 36–39 (2017).
- ¹⁰A. A. Kosterev, Y. A. Bakhrkin, R. F. Curl, and F. K. Tittel, "Quartz-enhanced photoacoustic spectroscopy," *Opt. Lett.* **27**, 1902–1904 (2002).
- ¹¹M. Lassen, L. Lamard, Y. Feng, A. Peremans, and J. C. Petersen, "Off-axis quartz-enhanced photoacoustic spectroscopy using a pulsed nanosecond mid-infrared optical parametric oscillator," *Opt. Lett.* **41**, 4118–4121 (2016).
- ¹²T. Steinle, F. Neubrech, A. Steinmann, X. Yin, and H. Giessen, "Mid-infrared Fourier-transform spectroscopy with a high-brilliance tunable laser source: Investigating sample areas down to 5 μm diameter," *Opt. Express* **23**, 11105–11113 (2015).
- ¹³T. Steinle, F. Mörz, A. Steinmann, and H. Giessen, "Ultra-stable high average power femtosecond laser system tunable from 133 to 20 μm ," *Opt. Lett.* **41**, 4863–4866 (2016).
- ¹⁴F. J. Harren, J. Mandon, and S. M. Cristescu, "Photoacoustic spectroscopy in trace gas monitoring," in *Encyclopedia of Analytical Chemistry*, edited by R. A. Meyers (John Wiley & Sons, Ltd., Chichester, UK, 2006).
- ¹⁵R. V. Kochanov, I. E. Gordon, L. S. Rothman, P. Wcisło, C. Hill, and J. S. Wilzewski, "HITRAN Application Programming Interface (HAPI): A comprehensive approach to working with spectroscopic data," *J. Quant. Spectrosc. Radiat. Transfer* **177**, 15–30 (2016).
- ¹⁶*Optik*, edited by E. Hecht and K. Lippert (Walter de Gruyter GmbH & Co. KG Verlag, Berlin; Boston, 2018), p. 17.
- ¹⁷Y. Saalberg, H. Bruhns, and M. Wolff, "Photoacoustic spectroscopy for the determination of lung cancer biomarkers—A preliminary investigation," *Sensors* **17**, 210 (2017).